

# Surface Modification of Polytetrafluoroethylene via Laser-induced Plasma Etching (LIPE)

Visar Demiri<sup>1</sup>, Martin Ehrhardt<sup>1</sup>, Pierre Lorenz<sup>1</sup>, Robert Heinke<sup>1,2</sup>, and Klaus Zimmer<sup>1\*</sup>

<sup>1</sup>Leibniz Institute of Surface Engineering (IOM), Permoserstr. 15, 04318 Leipzig, Germany

<sup>2</sup>Institute of Manufacturing Science and Engineering, Technische Universität Dresden, 01062 Dresden, Germany

Laser-induced plasma etching (LIPE) offers a promising technique for high-quality surface processing under atmospheric pressure. This study investigates the surface modification of polytetrafluoroethylene (PTFE) in air using a high-repetition-rate ultrashort pulsed laser. Key process and laser parameters, including repetition rate, pulse energy, plasma-to-surface distance, and etching time, were analyzed for their impact on etching rates and surface morphology. The etching rate of PTFE under stationary conditions was measured in the picometer-per-pulse range, enabling precise vertical control. Results show that etching rates increase with increasing pulse energy and repetition rate but decrease with greater plasma-to-surface distances. The generated etch grooves are circular and significantly larger than the laser spot size, with etched surfaces exhibiting reduced surface roughness compared to unetched surfaces. Line pattern etching was demonstrated by moving the sample at a constant speed in front of the laser-induced plasma. Unlike laser ablation, LIPE achieves superior vertical depth precision and significantly smoother surface morphology, making it a valuable tool for ultra-precise surface machining applications.

DOI: 10.2961/jlmn.2025.01.2010

**Keywords:** dry etching, plasma, laser, Polytetrafluoroethylene, surface modification, reactive etching, optical breakdown, laser-induced plasma etching, LIPE

## 1. Introduction

Ultra-precise surface machining (UPSM) is critical for advanced applications in electronics, optics and precision engineering. Achieving the surface quality required for such applications requires careful control of parameters such as surface roughness, subsurface damage, and depth precision, while balancing process speed, efficiency, and cost. Traditional UPSM techniques such as ion beam etching (IBE) and reactive ion beam etching (RIBE) are effective but limited by the need for a vacuum environment, which can reduce flexibility and increase operational complexity, especially for large or irregularly shaped substrates [1, 2]. In addition, these techniques are often used in combination with lithography processes to achieve the desired microscale patterning. Emerging atmospheric pressure techniques, including atmospheric pressure plasma jet (APPJ) processing and laser ablation, offer increased flexibility and direct writing capability, eliminating the need for complex vacuum setups [1-3]. Laser ablation, which has been widely applied to various materials in microelectronics and optics, relies on focusing the laser beam onto the substrate surface to induce material removal through absorption of laser photons via e.g. bond breaking, melting, vaporization, and explosion processes [4, 5]. However, laser ablation often results in increased surface roughness and subsurface damage. With typical ablation rates of 10 - 100 nm per pulse [6], its precision is often insufficient for ultra-high precision applications in optics and fine mechanics.

A promising alternative to laser ablation is laser-induced plasma etching (LIPE), which combines the flexibility of laser processing with the high precision of plasma etching. In LIPE, ultrashort laser pulses are focused in a reactive gas environment, inducing optical breakdown and creating a

localized microplasma [7]. This plasma generates reactive species that chemically interact with the surface to achieve high-precision etching. This method offers significant advantages by providing high depth control combined with low surface roughness.

The LIPE technique has shown promising results on various materials, including fused silica (SiO<sub>2</sub>), silicon (Si), germanium (Ge), and polymers such as polyimide films [8-13], supporting its applicability in microelectronics, aerospace, and biomedical fields. In this study, LIPE is applied to polytetrafluoroethylene (PTFE), a fluoropolymer known for its chemical inertness, low surface energy, and thermal stability, which make it ideal for high performance applications. However, these same properties, such as chemical inertness, make precision processing a challenge. The choice of this sample material is intended to demonstrate the versatile application potential of the LIPE process. This study investigates the influence of various laser parameters, including pulse energy, laser pulse repetition rate, and number of laser pulses applied, on the material removal rate. Furthermore, the possibility of complex surface patterning of PTFE by LIPE is demonstrated on an exemplary line pattern.

## 2. Experimental Details

An ultrashort laser pulse source was used to generate the laser-induced plasma for etching. This is done by focusing the ultrashort laser pulses through a lens to achieve the high field strength at the focal point required for optical breakdown and subsequent plasma ignition [5]. Figure 1 shows a sketch of the experimental setup. The laser source (PHAROS, PH2-20W) delivers ultrashort laser pulses with a wavelength of  $\lambda = 1030$  nm and a pulse duration of  $\tau_p = 260$  fs. The laser pulse repetition rate  $f_{rep}$  was varied

between 1 kHz and 50 kHz and the maximum pulse energy used was 400  $\mu\text{J}$ . The focal length of the lens used was  $f_{\text{opt}} = 12 \text{ mm}$ .

The beam diameter at the focal point was calculated by  $S = 2w_0 = \frac{4M^2\lambda f_{\text{opt}}}{\pi D}$  and the Rayleigh length by  $z_r = \frac{\pi w_0^2}{M^2\lambda}$ , with  $D$  (beam diameter,  $D = 4 \text{ mm}$ ),  $M^2$  (beam quality factor,  $M^2 = 1.2$ ), and  $w_0$  (Gaussian radius) [14]. The calculated values for the focal point spot size were  $S = 4.7 \mu\text{m}$  and the Rayleigh length  $z_r = 14.2 \mu\text{m}$ , respectively.

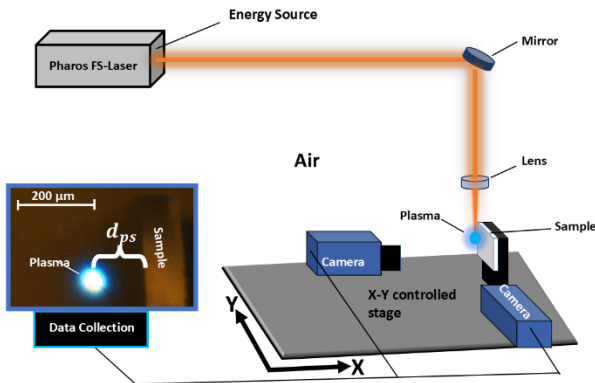


Fig.1 Experimental setup for laser-induced plasma etching.

In order to avoid direct laser irradiation of the sample, the sample surface was aligned parallel to the laser beam propagation direction as shown in Figure 1. Air at room temperature and atmospheric pressure was used as the etching gas. A computer-controlled X-Y-Z stage system was used to move the sample surface relative to the plasma. Two CCD cameras were installed to simultaneously image the LIP, the etch grooves, and the sample surface. The distance between the sample surface and the center of the visible laser-induced plasma was defined as the plasma-surface distance  $d_{ps}$ , which is determined by the cameras and can be adjusted by the stages. This plasma-surface distance was measured with an accuracy of  $\approx 5 \mu\text{m}$ . The stage accuracy is approximately  $1 \mu\text{m}$ . Polytetrafluorethylene (PTFE) sheets with a thickness of 2 mm and a size of 5 mm x 3 mm were used as samples. After the LIPE process, the surface of the PTFE is imaged by optical microscopy (OM), white light interferometry (WLI). In addition, scanning electron microscopy (SEM) was used to image the surface in more detail.

### 3. Results

With LIPE on PTFE, etching of the surface could be achieved and etching grooves are formed. Figure 2 shows an etching groove with a diameter of approx. 700  $\mu\text{m}$ . This groove was generated using an etching time of  $t = 21 \text{ min}$ , which corresponds to an applied laser pulse number  $N$  of  $N = 6.3 \times 10^7$ , calculated as  $N = \text{time} \times f_{\text{rep}}$ . Figure 2 a) shows a 3D contour plot measured by WLI, while Figure 2 b) shows the same etch groove imaged by SEM. The arrows in the figures indicate the direction of the laser beam propagation during the etching process. The etched groove has a circular-like shape.

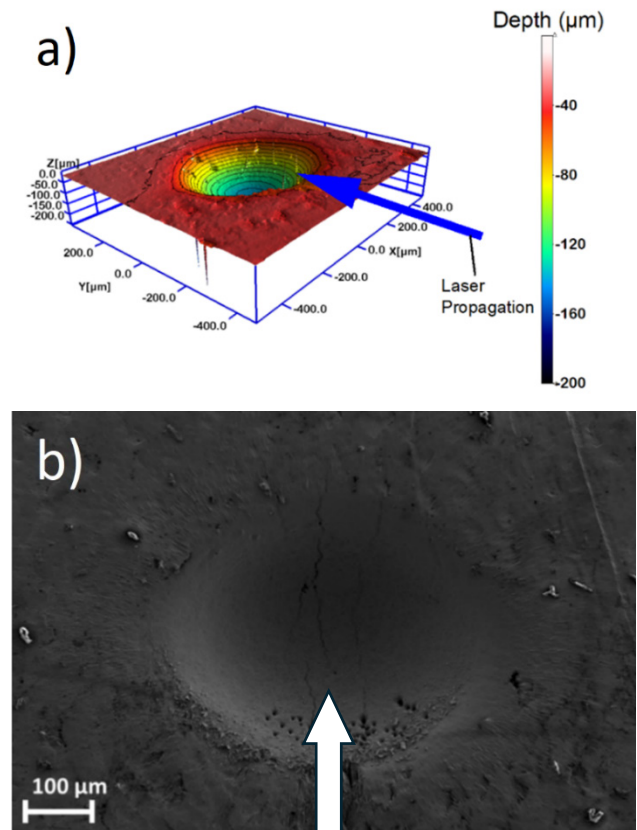


Fig. 2 a) 3D plot an etching groove measured by WLI. b) SEM image of the same groove. Etching parameters:  $t = 21 \text{ min}$ ,  $E = 380 \mu\text{J}$ ,  $d_{ps} = 120 \mu\text{m}$ ,  $f_{\text{rep}} = 50 \text{ kHz}$  and  $N = 6.3 \times 10^7$ . The arrows indicate the direction of the laser beam.

Cross-sections of etching grooves generated at different etching times are shown in Figure 3. It can be seen that the shape of the etching grooves is similar for the different etching times, while the depth and lateral size increase with increasing etching time. For the longest etch time studied ( $t = 21 \text{ min}$ ), the diameter of the etch groove was  $775 \mu\text{m} \pm 34 \mu\text{m}$ . This dimension of the etch footprint is more than two orders of magnitude larger than the calculated spot size of the laser beam at the focal point. This difference between the laser spot size and the etch groove indicates that the etch footprint is not correlated to the laser spot size, but to the involved plasma dynamics, which expands after the laser-induced optical breakdown [7, 15].

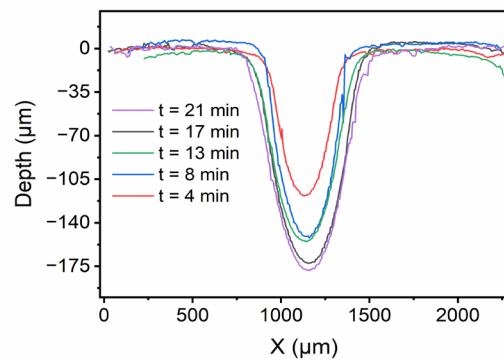
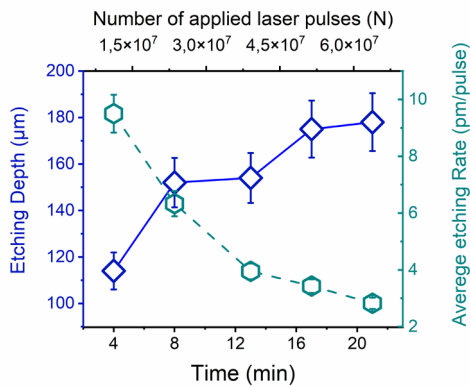


Fig. 3 Cross-sections of etched grooves generated with different etching times are shown. The etching parameters are

$E \approx 380 \mu\text{J}$ ,  $d_{ps} = 120 \mu\text{m}$ ,  $f_{rep} = 50 \text{ kHz}$ , and  
 $t = 4, 8, 13, 17, 21 \text{ min}$ .

Figure 4 shows the etching depth as a function of etching time. The etching depth increases as the etching time increases. For etching times of 4 min and 21 min, etching depths of  $114 \mu\text{m} \pm 9 \mu\text{m}$  and  $178 \mu\text{m} \pm 21 \mu\text{m}$  were achieved, respectively. Additionally, the averaged etching rate  $Y$  was determined by dividing the maximum measured etching depth by the applied laser pulse number  $N$ . For the  $t = 4 \text{ min}$ , an etching rate of  $Y = 9.5 \text{ (pm/pulse)} \pm 0.6 \text{ (pm/pulse)}$  was obtained, and for the  $t = 21 \text{ min}$ , an etching rate of  $Y = 2.8 \text{ (pm/pulse)} \pm 1.1 \text{ (pm/pulse)}$  was obtained. The trend found was that the etching rate decreases with increasing etching time.



**Fig. 4** Etching depth ( $\mu\text{m}$ ) and etching rate (pm/pulse) as a function of etching time (min). Etching parameters:  $E = 380 \mu\text{J}$ ,  $f_{rep} = 50 \text{ kHz}$ ,  $d_{ps} = 120 \mu\text{m}$ .

Figure 5 a) shows the correlation between the plasma-to-surface distance  $d_{ps}$  and the etching rate. For a plasma-to-surface distance of  $d_{ps} = 100 \pm 10 \mu\text{m}$ , an etching rate of  $Y = 8.9 \pm 0.6 \text{ (pm/pulse)}$  was obtained. The total number of pulses applied in this case was  $N = 1.2 \times 10^7$  for an etching time of  $t = 4 \text{ min}$ . The etching rate shows a linear dependence on the plasma-surface distance within the investigated parameter range. The linear fit to the etching rate  $Y \text{ (pm/pulse)} = a \times d_{sp} \text{ (}\mu\text{m)} + b$  yields the slope  $a = -0.0025 \pm 0.002 \text{ (pm/(pulse} \times \mu\text{m))}$ , and the intercept  $b = 10.9 \pm 0.6 \text{ (pm/pulse)}$ . This small etching rate underlines that within an etching cycle (- a laser pulse -) less than an atom size is removed in average.

Figure 5 b) shows the etching rate in dependence on the laser pulse energy and a linear dependence of the etching rate on the laser pulse energy is obtained. For a laser pulse energy of  $E = 380 \mu\text{J}$ , an etching rate of  $Y = 9.4 \pm 0.7 \text{ (pm/pulse)}$  is observed and for laser pulse energy of  $E = 150 \mu\text{J}$ , etching rate of  $Y = 1.5 \pm 0.1 \text{ (pm/pulse)}$  is obtained. The increase of the etching rate can be described by the linear fit of the etching rate with  $Y \text{ (pm/pulse)} = a \times E \text{ (}\mu\text{J)} + b$  yields the slope  $a = 0.03 \pm 0.002 \text{ (pm/(pulse} \times \mu\text{J))}$ , the intercept  $b = -2.4 \pm 0.4 \text{ (pm/pulse)}$ .

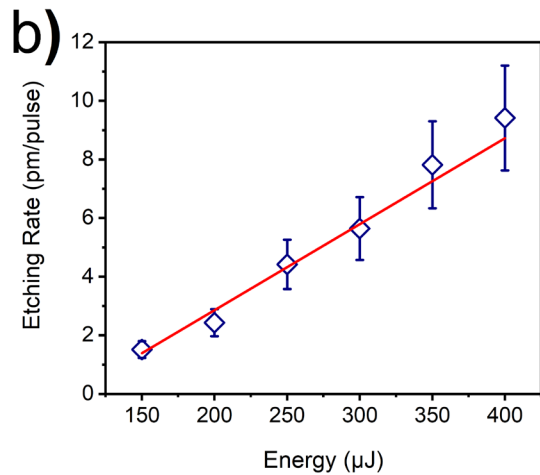
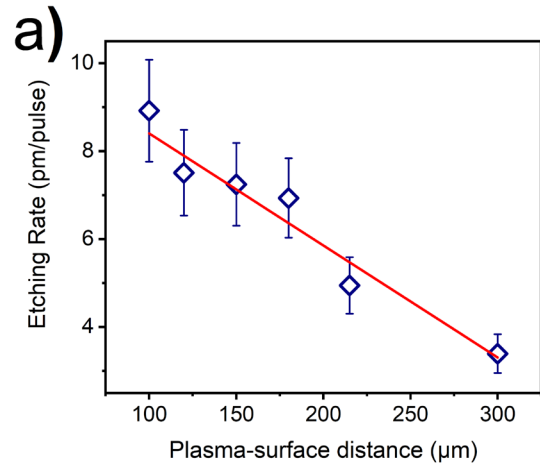


**Fig. 5 a):** Etching rate (pm/pulse) in dependence to plasma-surface distance ( $\mu\text{m}$ )  $d_{ps}$ . Etching parameters:  $t = 4 \text{ min}$ ,  $E = 380 \mu\text{J}$ ,  $f_{rep} = 50 \text{ kHz}$ ,  $N = 1.2 \times 10^7$ .

**b)** Etching rate (pm/pulse) in dependence to laser pulse energy ( $\mu\text{J}$ ). Etching parameters:  $t = 4 \text{ min}$ ,  $d_{ps} = 120 \mu\text{m}$ ,  $f_{rep} = 50 \text{ kHz}$ ,  $N = 1.2 \times 10^7$ .

The influence of the laser pulse repetition rate on the etching rate was also investigated (see Figure 6). For these experiments, the number of laser pulses applied was kept constant to make the results comparable. Therefore, the etching time was adjusted according to the laser pulse repetition rate. Figure 6 shows the measured dependence of the etching rate on the laser pulse repetition rate. As can be seen in this graph, a linear correlation was found between the etching rate and the laser pulse repetition rate. The experimental data shown in Figure 6 were fitted to a linear equation  $Y \text{ (pm/pulse)} = a \times f_{rep} \text{ (kHz)} + b$  yielding a slope  $a = 0.1 \pm 0.01 \text{ (pm/(pulse} \times \text{kHz))}$ , and a intercept of  $b = 3.5 \pm 0.03 \text{ (pm/pulse)}$ . (The virtual etching rate of 3.5 pm/pulse without laser action may be related to an experimental uncertainty or a nonlinear dependence on laser pulse repetition that is not covered by the parameter range investigated).

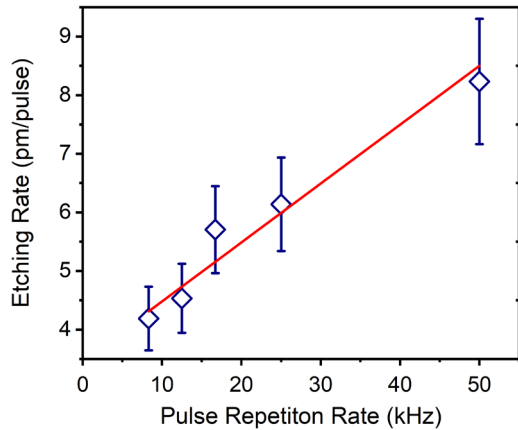


**Fig. 6** Etching rate (pm/pulse) dependent on laser pulse repetition rate. Etching parameters:  $E = 380 \mu\text{J}$  and  $d_{ps} = 120 \mu\text{m}$ . The total number of laser pulses applied,  $N = 1.2 \times 10^7$ , was kept constant by adjusting the etching time between  $t = 4$  and  $21$  min.

In order to demonstrate complex surface patterning, the sample was moved relative to the plasma position with a constant velocity  $v(x) = 0.05$  mm/s, keeping the distance  $d_{ps} = 100 \pm 5 \mu\text{m}$  constant throughout the etching. Figure 7a shows a WLI image of the generated trench. The depth of the trench was  $20 \pm 1.3 \mu\text{m}$  for the etching parameters used. The etched trench has a constant depth and a smooth surface as shown in the SEM of Figure 7b. No signs or features of melting were observed on the etched trench in the SEM image.

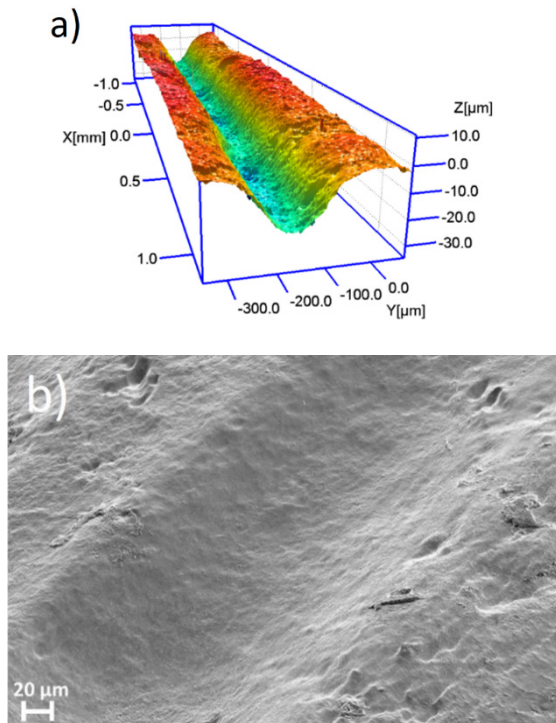


**Fig. 7** a) 3-dimensional contour plot of the etched line measured with WLI. b): SEM image of the LIPE etched line. Constant etching parameters:  $v(x) = 0.05$  mm/s,  $E = 380 \mu\text{J}$ ,  $d_{ps} = 100 \mu\text{m}$ ,  $f_{rep} = 50$  kHz.

#### 4. Discussion and conclusions

The Laser-Induced Plasma Etching (LIPE) of Polytetrafluoroethylene (PTFE) was performed at air, under atmospheric pressure and at room temperature. The air with the main components oxygen and nitrogen was utilized as etchant gas. Plasma's energy source was an ultrashort pulsed laser operating at a repetition rate ranging from 1 to 50 kHz. The laser beam is focused into the air where optical breakdown cause the plasma ignition once the energy density exceeds a critical value [5, 16-18]. The excited reactive species formed in the plasma, such as the free radicals, reactive species and ions, react with the PTFE's surface, breaking directly bonds of PTFE or initiating chemical reactions with the surface atoms which results in the formation of volatile products and in consequence causing a material removal. Due to air being used as the etchant gas, reactive oxygen is the dominating etchant of the surface; slight contributions from excited nitrogen and hydrogen compounds may occur too [5, 19, 20]. Chemically, the polytetrafluoroethylene consists of an aliphatic backbone where the hydrogen is substituted by fluorine. The most likely mechanism of attack on the PTFE surface by reactive oxygen results in the formation of carbonyl, hydroxyl, and aldehyde groups replacing the fluorine atoms [21]. Continuing chemical oxidation cause the formation of volatile products such as F atoms, volatile fluorine containing molecules and  $\text{CO}_2$  increasingly [22]. Also the creation  $\text{CF}_x$  reaction products needs to be considered [19, 22].

In the case of a fluorocarbon surface, as in the investigated PTFE, slow plasma etching rates are characteristic, in comparison with other polymers containing fluorine [2]. It must be noted that the surface temperature is increased by the interaction of the LIP with the surface. However, it can be assumed that the resulting temperature is lower than the melting point of PTFE, since no features typically associated with melting were observed (see e.g. Figure 2b) and Figure 7b), so it can be concluded that thermal decomposition of PTFE is not the main mechanism of material removal, while chemical etching can also be assumed below the melting point. The LIP can additionally generate UV and X-rays which can assist the chemical reactions as well as adsorption and desorption processes [23, 24]. Therefore, in the LIPE is determined by a complex mechanism with diverse linked processes of species generation species transport, chemical etching and material removal. The material removal of LIPE process produces etch grooves. The etching depth and etching rate depend on the laser parameters (such as laser-energy, -pulse time, -pulse repetition rate) or experimental conditions e.g. the plasma-surface distance  $d_{ps}$ .

The influence of the plasma – surface distance was investigated, and the results are shown in figure 5a. The observed decrease in the etching rate by increasing the plasma – surface can be explained by several factors. 1) The mean free path length in these experiments is roughly 3 orders of magnitude smaller than the plasma's distance to the surface [19]. This short mean free path length facilitates numerous collisions and interactions among plasma species during diffusion. Such interactions may cause reactive species to be consumed through side reactions or radicals to become

deactivated. As the distance increases, the frequency of collisions grows, leading to a reduction in the number of reactive fluorine radicals reaching the surface. Consequently, this results in decreased etching rates. II) The diffusion of reactive species is time-dependent and is expected to exhibit an  $R^2$  dependence, as the laser-induced plasma functions as a point source of radicals driven by the laser. However, as shown in figure 5a, the experiments revealed a linear relationship between the etching rate and the plasma-surface distance. This indicates that the experimentally observed plasma-distance dependence cannot be fully explained by transport processes such as radical flow and diffusion. Nevertheless, an increase in the plasma-surface distance is anticipated to result in a decrease in the density of reactive species reaching the surface. Figure 4 shows that the etching rate decreases with increasing etching time and depth. This trend of decreasing etching rate with increasing etching time was also observed in the other LIPE experiments [8-13, 16, 25]. The decrease in etching rate was explained by the increasing distance between the surface and the plasma during etching. The longer distance from the plasma to the surface causes an increase in the diffusion time and travel distance of the reactive species, resulting in a deactivation of the reactive species by collisions. Furthermore, the reduction in the area density of reactive species and emitted photons is related to geometrical effects, as already discussed.

The plasma volume, proportional to the number of available reactive species, depends on the laser pulse energy and the focal length [15]. As the laser pulse energy increases, the plasma volume expands, producing more reactive species for chemical etching. Additionally, higher pulse energy generates denser, more highly excited plasma, which further enhances the availability of reactive species. This relationship, as shown in figure 5b, results in an increased etching rate at higher laser-pulse energies, consistent with findings from other studies [12, 13]. The plasma transfers heat to the sample surface through interactions with reactive species and radiation. Larger plasma volumes, produced by higher pulse energy, increase heat transfer, raising the surface temperature. Similarly, the laser pulse repetition rate affects heating: at higher repetition rates, the surface has less time to cool between pulses, leading to higher surface temperatures. This cumulative heating effect, illustrated in figure 6, also contributes to increased etching rates.

In previous studies on LIPE, it was shown that the processing of various materials, including silicon (Si), polymers, germanium (Ge), and silicon dioxide ( $\text{SiO}_2$ ), is feasible [10, 11, 13, 8]. The reported characteristic etching rates were 117 pm/pulse for Si, 70 pm/pulse for polyimide, 75 pm/pulse for Ge, and 25 pm/pulse for  $\text{SiO}_2$ . These rates are significantly higher than those observed in this study, which ranged from 1 to 10 pm/pulse. Several factors explain this difference. Most prior studies employed ultrashort laser pulses with low repetition rates but high pulse energies. Additionally, external heating was often applied during the LIPE process in these studies, which is known to enhance the etching rate.

Despite these differences, the general etching behavior remains consistent across studies. For example, etching rates exhibit a linear dependency on parameters such as laser pulse energy and plasma-to-surface distance.

The etching groove shown in Figure 2 exhibits a circular like shape, corresponding to the visible plasma emission observed in the camera view (see Figure 1). This observation, combined with the fact that the etching groove is more than two orders of magnitude larger than the laser beam's focal spot size, suggests that the material removal process is governed primarily by plasma dynamics following optical breakdown, rather than by direct laser interaction with the surface.

The very low ablation per applied laser pulse makes the LIPE technique particularly suitable for I) the correction or refinement of high-quality surfaces and II) the removal of thin layers without damaging the underlying layers of a sample.

### Acknowledgments and Appendixes

The work was funded by the Deutsche Forschungsgemeinschaft (DFG, German Research Foundation) – 453925455 (ZI 660/22-1 and AR817/7-1). The authors thank I. Mauersberger for assistance with SEM imaging and topographic analysis of the structures.

### References

- [1] T. Arnold, G. Boehm, and A. Schindler: *J. Vac. Sci. Technol. A*, 19, (2001) 2586.
- [2] H. Paetzelt, G. Böhm, and T. Arnold: *Plasma Sources Sci. Technol.*, 24, (2015) 025002.
- [3] I.M. Eichentopf, G. Böhm, J. Meister, and T. Arnold: *Plasma Process. Polym.*, 6, (2009) S204.
- [4] A.A. Serafetinides, M.I. Makropoulou, C.D. Skordoulis, and A.K. Kar: *Appl. Surf. Sci.*, 180, (2001) 42.
- [5] W. Hu, Y.C. Shin, and G. King: *Appl. Phys. Lett.*, 99, (2011) 234104.
- [6] W. Hu, Y.C. Shin, and G. King: *Appl. Phys. Lett.*, 99, (2011) 234104.
- [7] A.M. Hossain, M. Ehrhardt, M. Rudolph, D. Kalanov, P. Lorenz, K. Zimmer, and A. Anders: *J. Phys. D: Appl. Phys.*, 55, (2021) 125204.
- [8] M. Ehrhardt, P. Lorenz, B. Han, and K. Zimmer: *Appl. Phys. A*, 126, (2020) 842.
- [9] K. Zimmer, M. Ehrhardt, P. Lorenz, X. Wang, P. Wang, and S. Sun: *Ceram. Int.*, 48, (2021) 90.
- [10] R. Heinke, M. Ehrhardt, P. Lorenz, and K. Zimmer: *Appl. Surf. Sci. Adv.*, 6, (2021) 100169.
- [11] M. Ehrhardt, P. Lorenz, J. Bauer, R. Heinke, M.A. Hossain, B. Han, and K. Zimmer: *Lasers Manuf. Mater. Process.*, 8, (2021) 237.
- [12] V. Demiri, M. Ehrhardt, P. Lorenz, R. Heinke, and K. Zimmer: *Appl. Surf. Sci. Adv.*, 17, (2023) 100450.
- [13] L. Streisel, M. Ehrhardt, P. Lorenz, R. Heinke, A. Hossain, and K. Zimmer: *J. Laser Micro Nanoeng.*, 17, (2022) 28.
- [14] N. Lindlein and G. Leuchs: "Springer handbook of lasers and optics" ed. by F. Träger (Springer, 2012), p. 151.
- [15] A.M. Hossain, M. Ehrhardt, M. Rudolph, P. Lorenz, D. Kalanov, K. Zimmer, and A. Anders: *ACS Photonics*, 10, (2023) 1232.
- [16] M. Ehrhardt, P. Lorenz, and K. Zimmer: "Ultrafast Laser Nanostructuring: The Pursuit of Extreme Scales" ed. by R. Stoian and J. Bonse (Springer, 2023), p. 653.
- [17] C.G. Morgan: *Rep. Prog. Phys.*, 38, (1975) 621.

- [18] P. Belland, C. De Michelis, and M. Mattioli: *Opt. Commun.*, 4, (1971) 50.
- [19] A. Fridman: *Plasma Chem.*, Cambridge Univ. Press, 2008.
- [20] R. Tambay and R.K. Thareja: *J. Appl. Phys.*, 70, (1991) 2890.
- [21] C. Liu, R. Arnell, A. Gibbons, S. Green, L. Ren, and J. Tong: *Surf. Eng.*, 16, (2000) 215.
- [22] M. Morra, E. Occhiello, and F. Garbassi: *Surf. Interface Analy.*, 16, (1990) 412.
- [23] N.S. Allen: *Photochem.*, 34, (2007) 197.
- [24] J. Guillet: "Polymer photophysics and photochemistry. An introduction to the study of photoprocesses in macromolecules" (Cambridge University Press, Cambridge, 1985), p. 347.
- [25] K. Zimmer, M. Ehrhardt, and R. Böhme: "Laser Ablation in Liquids: Principles and Applications in the Preparation of Nanomaterials" ed. by G. Yang (Pan Stanford Publishing, Singapore, 2012), p. 129.

(Received: January 3, 2025, Accepted: March 24, 2025)